Probing Heavy Spin-2 Bosons with $\gamma\gamma$ final states from Vector Boson Fusion Processes at the LHC

written by

Yuhan Guo

under the supervision of **Prof. Alfredo Gurrola**, and submitted to the Faculty of the Department of Physics and Astronomy of Vanderbilt University in partial fulfillment of the requirements

for

DEPARTMENTAL HONORS

in

PHYSICS

Date of the public defense:
April 19, 2019

Members of the Thesis Committee:
Prof. Alfredo Gurrola
Prof. Will Johns
Prof. Paul Sheldon
Prof. Richard Haglund

Additional thanks to Savanna Starko for her mentoring.

Abstract

New massive spin-2 particles are predicted in theoretical extensions to the Standard Model (SM) attempting to solve the hierarchy problem. Such theories postulate that gravity is diluted compared to the other fundamental forces because it can propagate in extra spatial dimensions. While such theoretical models are of high experimental interest because they predict massive spin-2 particles (Y_2) potentially detectable by collider experiments, searches at the Large Hadron Collider (LHC) have thus far produced no significant evidence for their existence. This work considers a hypothetical physics scenario where low coupling strengths between the Y_2 and quarks/gluons is the underlying reason behind the null Y_2 search results at the LHC, which have mainly relied on Drell-Yan and gluon-gluon fusion production mechanisms. The focus of this paper is a feasibility study to search for Y_2 particles using vector boson fusion (VBF) processes at the LHC. In the context of an effective field theory approach with varying couplings κ_V between Y_2 and the weak bosons of the SM, we consider the $Y_2 \to \gamma\gamma$ decay mode to show that the requirement of a diphoton pair combined with two high p_T forward jets with large dijet mass and with large separation in pseudorapidity can significantly reduce the SM backgrounds. Assuming proton-proton collisions at $\sqrt{s} = 13$ TeV, we present the total VBF production cross sections, Y_2 decay widths, and $Y_2 \to \gamma\gamma$ branching ratios as a function of $m(Y_2)$, considering universal and non-universal couplings to the SM particles. The unitarity-violating phase space is described. The proposed VBF $Y_2 \to \gamma\gamma$ search is expected to achieve a discovery reach with signal significance greater than 5σ for Y_2 masses up to 4.4 TeV and κ_V couplings down to 0.5.

Contents

1 Introduction

The introduction to this thesis document is structured as follows. In Section 1.1, we outline the Standard Model (SM) by describing the included particles and the fundamental forces by which they can interact. The data from collider experiments offers a powerful tool to study these fundamental particles and their interactions, including the SM and potential new physics beyond our current framework/understanding. Thus, in Section 1.2, we describe the Large Hadron Collider (LHC) and the Compact Muon Solenoid (CMS) experiment, which are the experimental apparatus used to study these fundamental interactions. In particular, the detector parameters and performance of the CMS experiment are ultimately what we will simulate in the phenomenological analysis described in this thesis. In Section 1.3, we will provide further physics motivation behind our analysis.

1.1 Introduction to the Standard Model of Particle Physics

Everything in our universe is made from basic building blocks called fundamental particles, which are governed by four fundamental forces: the electromagnetic force, the strong force, the weak force, and gravity. Our best understanding of how particles and three of the forces (excluding gravity) are related to each other is described by a mathematical framework referred to as the Standard Model (SM) of particle physics.

All SM particles are either fermions, which are the building blocks of ordinary matter, or bosons, which are mediators of the fundamental interactions which bind fermions into what we typically refer to as the "ordinary matter" we see in our everyday world. Fermions have half-integer spin. In particular, the fundamental fermions of the SM have spin 1/2. Bosons have integer spins. The bosons of the SM include the spin-1 vector bosons (photon, gluon, W, and Z), and the spin-0 Higgs boson. As we will later discuss in more detail, the hypothetical particle called the graviton - mediator of gravitational interactions - has spin 2

but is not included in the SM of particle physics. Important properties of these fundamental particles, such as the spin number, charge and mass, are summarized in Table 1.

The SM fermions come in two types: quarks and leptons. As shown in Fig. 3, both quarks and leptons appear in three generations, where each subsequent generation is more massive than the previous. Quarks are also distinguished by their electric charge into six flavors: up (u), down (d), charm (c), strange (s), top (or truth; t) and bottom (or beauty; b). The up, charm and top quarks have an electric charge that is 2/3 that of the electron charge e, while the down, strange and bottom quarks have charge -1/3e. Though the fractional charge (in multiples of 1/3e) of quarks seems counter-intuitive, all composites of quarks and antiquarks - baryons made up of three quarks, and mesons made up of a quark and an antiquark - have integer charge. For instance, it is easy to check that all possible baryons one can make out of the up (u) and down (d) quarks are: uuu (with charge 2), uud (with charge 1; also called the "proton"), udd (with charge 0; also called the "neutron"), and ddd (with charge -1). Similarly, it is easy to check that all mesons have charge $\pm$ 1 or 0.

Besides flavor (uniquely determined by its generation and charge), each quark may have any of the following three possible color charges (or simply color): red, green and blue. However, quarks cannot be isolated (and hence cannot be observed individually), and all composites (baryons and mesons) of quarks and antiquarks existing in nature must be colorless - this phenomena is known as "color confinement." It is worth noting that the "colors" are not real colors but rather a classification scheme used in describing the strong interaction. The role of a quark's "color" (or "color charge") in strong interaction offers a convenient analogy to that of a particle's electric charge in the electromagnetic interaction. Quarks make up baryonic matter, including all atoms in the universe, accounting for 5% of all the mass of the universe [1].

Leptons are classified by their electron number (L_e), muon number (L_μ) and tau number (L_τ) into three generations (or "weak pairs," as each lepton can be changed to its "paired

partner" via charged weak interaction), with the two in each pair further distinguished by the charge: electron, muon and tau have charge -1 while their corresponding neutrinos have zero charge.

In modern particle physics, the fundamental particles interact through four fundamental forces, summarized in Table 2: the strong, electromagnetic, weak, and gravitational forces. Only the first three are included in the SM. The SM includes four vector bosons: the gluon, photon, $W^{\pm}$ boson and Z boson. They are mediators of these three fundamental interactions: for instance, the familiar electromagnetic force between two electrons can be thought of as being "mediated" by exchange of photons between the electrons.

The strong force acts on all the quarks and is mediated by gluons. A gluon has no mass or charge and carries both one "color" and one "anticolor." During the strong interaction, the colors of the participant quarks may change, in which case the color difference is carried away by the mediating gluon. At the scale smaller than a femtometer (fm), the strong force is the strongest of the four fundamental forces, and it holds together the three quarks making up a proton or a neutron. For larger scales of 1-3 fm, the strong force binds protons and neutrons to form nuclei [2]. The strong force shows an interesting characteristic: it becomes vanishingly weak as the quarks are close and grows stronger at large distances. In particular, it takes infinitely high energy to pull apart one quark from a hadron, explaining why we never observe an individual/isolated quark. On the other hand, at very high energies (small distances), the strong force is vanishingly (or asymptotically) weak so that quarks become free particles. This feature of the strong force is known as asymptotic freedom.

The electromagnetic force acts on all the SM fermions with nonzero electric charge (i.e, all SM fermions except for neutrinos), where particles with opposite electric charges attract and those with the same electric charge repel. The electromagnetic force is mediated by photons, which have no mass, charge, or color. Photons make up electromagnetic waves, with frequencies ranging from radio waves to gamma ray. The electromagnetic force has

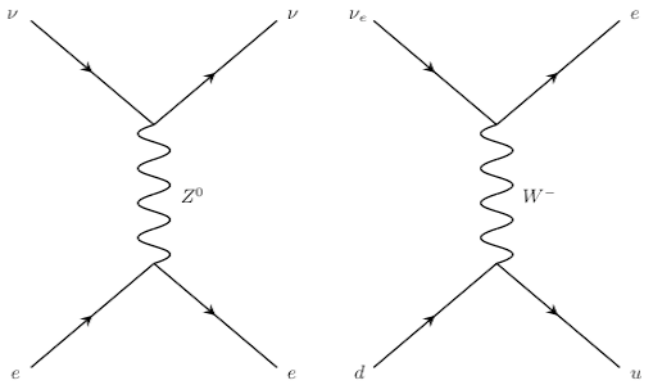

Figure 1: Feynman diagrams of two examples of the weak interaction, in which time flows from left to right. Shown on the left panel is a neutrino scattering off an electron ($e + \nu \rightarrow e + \nu$, where the neutrino ν can be in any generation), a neutral weak interaction. Shown on the right panel is the beta decay $d + \nu_e \rightarrow u + e$, a charged weak interaction.

infinite range, and its strength is proportional to the electric charges of the particles and to r^{-2}, where r is the distance between the particles.

The weak force acts on all quarks and leptons and has two types: (i) neutral, mediated by the Z boson; and (ii) charged, mediated by the W bosons. Note that the W and Z bosons are the only massive vector bosons. In a neutral weak interaction, mediated by the Z boson, two fermions come in, interact with each other, and "annihilate" to produce an intermediate Z boson, which then produces two fermions coming out as final state particles. Fig. 1 shows the Feynman diagrams of two examples of the weak interaction, in which time flows from left to right. Shown on the left panel of Fig. 1 is a neutrino scattering off an electron ($e + \nu \rightarrow e + \nu$, where the neutrino ν can be in any generation), a neutral weak interaction. Shown on the right panel is the beta decay $d + \nu_e \rightarrow u + e$.

The charged weak interaction is mediated by the W bosons, which have electric charge $+1e$ (W^+) or -1e (W^-). It changes a lepton into its partner lepton of the same generation (for instance, e to ν_e); for quarks, the charged weak interaction usually acts in the same way, changing a quark to its partner quark of the same generation, but "cross-generational" weak interactions also occur (for instance, changing a strange quark to an up quark). The

charge difference between the incoming lepton/quark and the outcoming one is carried away by the W boson. The weak force is weaker than both the electromagnetic and the strong forces, about five orders of magnitude weaker than the strong force at the scale of an atom's nucleus [3]. Yet it is important in processes such as beta decay and in the study of violation of parity (mirror symmetry).

Fig. 2 shows the so-called Higgs field, which is a scalar field with a Mexican-hat shape: it has a degenerate ground state and non-zero vacuum expectation value. Though all choices of ground state (related to each other by an $SU(2)$ gauge transformation) give the same physics, any choice of a ground state would result in a "distinguished direction" and simultaneously break the symmetry. This process of spontaneous breaking of the electroweak gauge symmetry is called the Higgs mechanism and explains why photons, mediators of the electromagnetic interaction, are massless, while the W and Z bosons, mediators of the weak interaction, have nonzero mass [7].

The Higgs mechanism predicts the existence of the Higgs boson, a particle with spin zero, no electric charge or color charge. Experimental detection of the Higgs boson can test the Higgs mechanism. In 2012, the ATLAS and CMS experiments at the LHC detected a new particle in the mass region around 125 GeV and confirmed it to be a Higgs particle - the signal observed at the LHC and the experimental measurements (e.g. mass and couplings) agreed well with the theoretical prediction of the Higgs mechanism, and deviated from the background by more than 5 standard deviations. François Englert and Peter Higgs, who proposed the Higgs mechanism, were awarded the 2013 Nobel Prize for the discovery of the Brout-Englert-Higgs mechanism [8].

The SM has been a successful theory, agreeing with decades of experimental observations involving the weak, electromagnetic, and strong forces. However, the SM remains an incomplete theory. As mentioned above, the most familiar force in our everyday lives, gravity, is not included in the Standard Model. In particle physics, the analogy with the other three

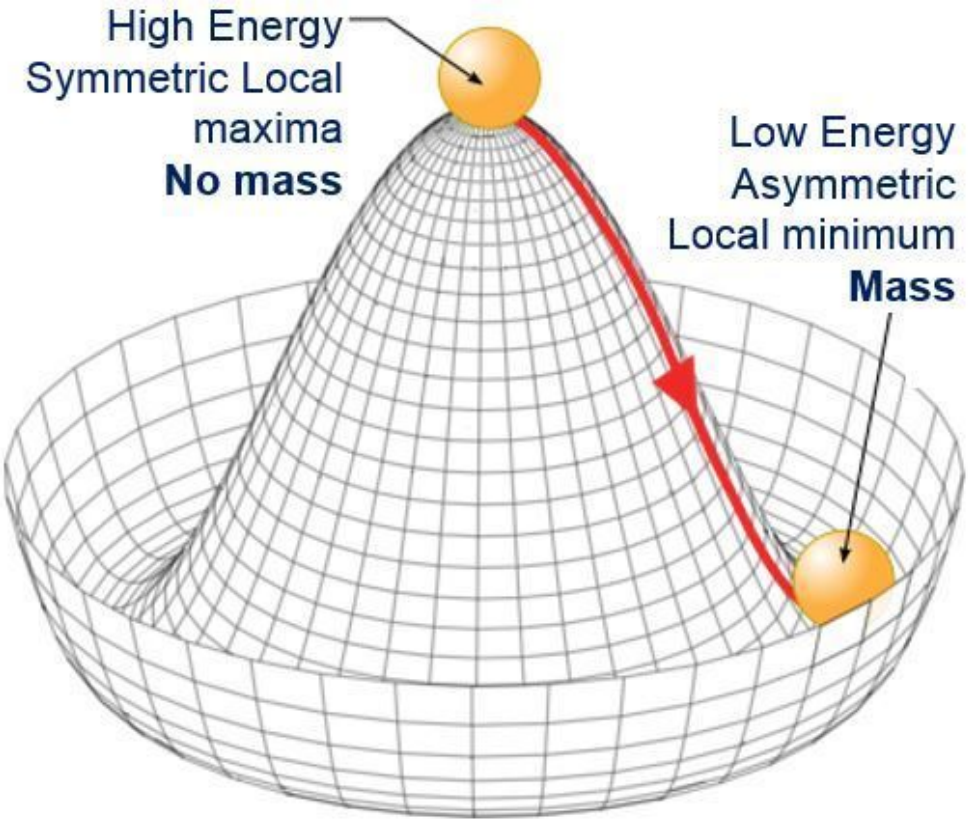

Figure 2: Illustration of the Higgs field and the process of spontaneous symmetry breaking. Image: [9].

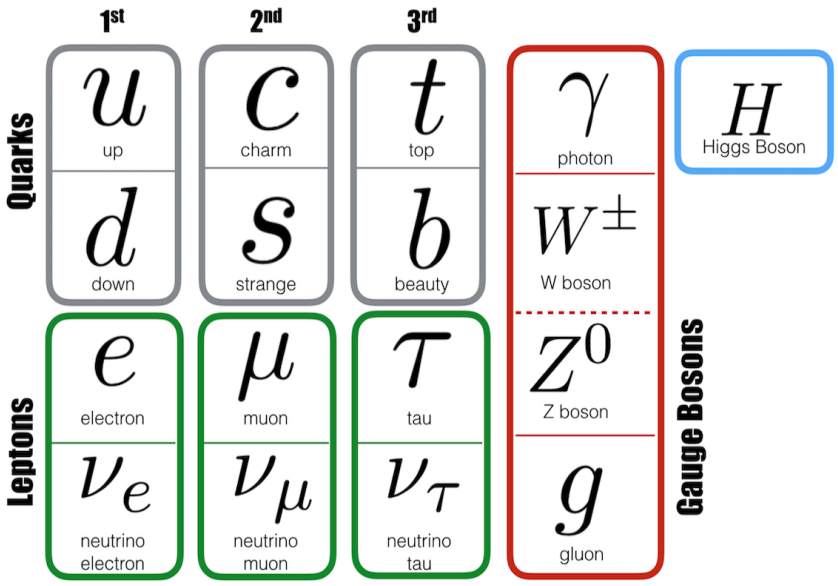

Figure 3: The Standard Model of particle physics. Image: [4]

.

forces indicates that the gravitational force, too, should have a mediator - known as the "Graviton." (The picture of a Graviton as in Einstein's theory of general relativity is a massless spin-2 particle, which is difficult to detect due to its zero mass.) The reason gravity is not incorporated in the SM is because its strength is diluted compared to the weak force, the weakest of the three interactions in SM, by order of 10^{29} [5]. This leads to the so-called hierarchy problem. Models with extra spatial dimensions offer one family of solutions to this problem. As we will see in the next subsection, these types of models, combined with the gravitational interaction, result in the manifestation of several spin-2 gravitons which range in mass from zero to several TeV. Since these massive TeV-scale gravitons do not exist "naturally" in nature, this motivates searching for these hypothetical particles in a very high energy environment such as the LHC.

Table 1: Information about the particles of the SM, including their main properties such as electric charge and spin, and the year in which they were predicted/discovered [6]

Family		Particle		Predicted	Discovered	Spin Number	Charge (e)	Color	Mass (MeV/c^2)
Fermions	Quark	u	up quark	1964	1968	1/2	+2/3	r,g,b	2.2
		d	down quark	1964	1968	1/2	-1/3	r,g,b	4.7
		c	charm quark	1970	1974	1/2	+2/3	r,g,b	1275
		s	strange quark	1964	1968	1/2	-1/3	r,g,b	95
		t	top quark	1973	1995	1/2	+2/3	r,g,b	173000
		b	bottom quark	1973	1977	1/2	-1/3	r,g,b	4180
	Leptons	e	electron	1874	1897	1/2	-1	none	0.51099895
		μ	muon		1936	1/2	-1	none	105.658375
		τ	tau		1975	1/2	-1	none	1776.86
		ν_e	electron neutrino	1930	1956	1/2	0	none	$< 10^{-7}$
		ν_μ	muon neutrino	1940s	1962	1/2	0	none	$< 10^{-7}$
		ν_τ	tau neutrino	1970s	2000	1/2	0	none	$< 10^{-7}$
Boson	Vector	g	gluon	1962	1978	1	0	8 colors	0
		γ	photon		1899	1	0	none	0
		W	W boson	1968	1983	1	± 1	none	80379
		Z	Z boson	1968	1983	1	0	none	91187.60
	Scalar	H	higgs boson	1964	2012	0	0	none	125180

Table 2: The four fundamental forces [5].

Force	Strength	Theory	Mediator
Strong	10	Chromodynamics	Gluon
Electromagnetic	10^{-2}	Electrodynamics	Photon
Weak	10^{-13}	Flavordynamics	W and Z
Gravitational	10^{-42}	Geometrodynamics	Graviton (not in SM)

1.2 Introduction to the Large Hadron Collider (LHC) & Compact Muon Solenoid (CMS)

The LHC is a proton-proton (pp) collider, where two circulating, high-energy beams of protons are accelerated to nearly the speed of light and collide, as shown in Fig. 4. In the remaining of this thesis, we denote as the z-axis the line tangent to the curves of the two incoming beams at the momentum of collision, and we call the transverse plane the xy-plane.

The LHC consists of a 27-kilometer ring of superconducting magnets, together with a number of accelerating structures along the tunnel for boosting the particles [11]. Since it began operation on the 10^{th} of September 2008, the Large Hadron Collider (LHC) at CERN has been the world's largest and most powerful particle collider [11]. Starting in 2010 with a total collision energy of 7 TeV, the LHC was upgraded to 8 TeV in 2012, and it is currently operating at total collision energy of 13 TeV, holding the world record [12]. We use the term *instantaneous luminosity* to denote the number of collisions produced in a detector per cm^2 and per second [14]. The integrated luminosity is the integral of instantaneous luminosity over the entire data-taking period. By 2018, the LHC has reached integrated luminosity of 150 fb^{-1}, where 1 $\text{fb}^{-1} = 10^{43}\ \text{m}^{-2} = 10^{39}\ \text{cm}^{-2}$ [13].

There are four particle detectors located along the LHC ring: the Compact Muon Solenoid (CMS) and ATLAS are general-purpose detectors, while ALICE and LHCb are specialized detectors serving studies of very specific phenomena. The experimental high energy physics group at Vanderbilt University is part of the CMS experiment, and therefore the remainder of this thesis focuses on discovery potential with the CMS detector.

The high energy (relativistic momentum) of the incoming beams allows creation of massive (including TeV scale) particles at the collision, where the momentum of the incoming partons, particles making up the protons, is transferred into rest mass energy (in particular the rest mass energy of a heavy spin-2 graviton). The heavy spin-2 gravitons of interest then

decay into stable, detectable SM particles. The CMS detector acts as a high-speed camera that takes pictures of these collisions from all angles up to 4×10^7 times per second, allowing for the study of an incredible amount of pp collision data [10].

The CMS detector is cylindrical in shape with dimensions of 21 meter long, 15 meters wide and 15 meters high [10]. Fig. 6 shows the different components of the CMS detector, including a huge superconducting solenoid magnet at the center, which bends all charged particles. Fit inside the solenoid are the silicon trackers, which trace the paths of the charged particles to measure their momenta, the crystal electromagnetic calorimeter (ECAL), which measures the energy of electrons and photons, and the hadron calorimeter (HCAL), which measures the energy of hadrons. The muon chambers lying at the outer edge of CMS detect muons by tracing their paths and measuring their momenta.

Weighing 12,000 tonnes, the solenoid magnet at CMS is the largest superconducting magnet ever built [10]. Thanks to the size of the magnet and the superconducting materials (hence zero resistance!), the CMS magnet creates a 4 Tesla magnetic field, which is 100,000 times stronger than the Earth's magnetic field [10]. This powerful magnetic field can bend the paths of charged particles traveling at relativistic speeds. The strong bending, combined with fine tracker segmentation, allows precise measurements of the particles' momenta [10].

The silicon tracker reconstructs the tracks of the charged particles. A particle passing through the tracker interacts with the silicon via the electromagnetic force and produces an electric signal. The signal is then amplified and detected via internal and external means of readout that communicate. Through this way, the tracker can very accurately measure the particle's position at several key points and thereby reconstruct its path. The tracker is designed to disturb the particle as little as possible [10].

By bending a charged particle and tracing its path, we can measure the charge and momentum of the particle. The sign of the charge determines the bending direction, while the magnitude of charge and the particle's momentum determine how much the particle

bends. To see this, let us consider the simple example of a charged point particle moving in arbitrary direction in the xy-plane of the three-dimensional Euclidean space (using Cartesian coordinates), while a constant magnetic field $\boldsymbol{B}$ points in the positive direction along the z-axis ($\boldsymbol{B} = B\hat{z}$). Denote absolute value of the charge of the particle as q, its mass as m. Denote the strength of the magnetic field as $B = |\boldsymbol{B}|$. With the magnetic force being the only force acting on the particle, the particle takes a circular motion in the xy-plane with constant speed (denoted v). If the charge is positive, the particle moves in a counterclockwise circle. If the charge is negative, the particle moves in a clockwise circle. The radius of the particle's orbit is given by $mv^2/R = qvB$; i.e, $R = mv/qB$. It is hence clear that the higher momentum p $(= mv)$ the particle has, the larger the radius of its circular orbit, hence the smaller the curvature of the orbit. In addition, the radius R is inversely proportional to absolute value of the charge of the particle. Hence, particles with higher charge and with smaller momentum bend more. Though this example is simple and idealized, the conclusions we get are general. The charge and momentum of a charged particle, which we can obtain from bending the charged particle and tracing its path, offer crucial information for determining the particle's identity [10].

CMS uses calorimeters to measure the energy of particles produced in the collision. The electromagnetic calorimeter (ECAL) measures the energy of electrons and photons by stopping them completely, via the electromagnetic interaction. The ECAL is built from lead tungstate crystals, a scintillating material. When electrons and photons hit the calorimeter, the ECAL produces fast and short photon bursts, which are then detected by photodetectors and analyzed [10].

The hadron calorimeter (HCAL) at CMS measures the energy of hadrons, composites made up of quarks and gluons, by completely stopping them and then analyzing the radiated pulses of light. The HCAL is a sampling calorimeter: it uses alternating layers of "absorbers" and scintillating materials for measurement. The layers produce rapid light pulses as a

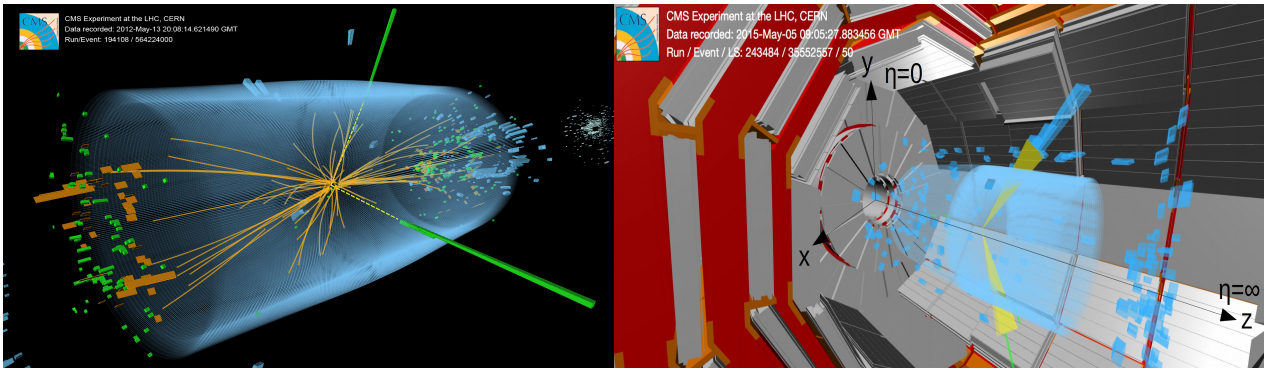

Figure 4: Proton proton collision at the large hadron collider (LHC). Definition of the x, y, z axes by convention.

hadron passes through. The light pulses are collected and transported by specific optical fibres into readout boxes, where photodetectors amplify/detect the signal. Summing the light signals over all the layers gives a measurement of the particle's energy [10].

Detection of muons is difficult since muons can "penetrate several meters of iron without interacting" [10]. Unlike other particles, muons are not stopped by any of the CMS calorimeters. As the name "Compact *Muon* Solenoid" suggests, muon detection is a main task of the CMS experiment. The CMS has 1,400 muon chambers for detection of muons. These chambers lie at the edge of the detector, where all other particles have been stopped by the calorimeters and are unlikely to penetrate. The path of a muon is traced by measuring its position at four muon stations and fitting a curve to these measurements. Since the CMS magnet is so powerful, it can bend even muons with very high energy, trace their paths, and measure their momenta [10].

1.3 Motivation

The most important physics result at the CERN Large Hadron Collider (LHC) to date is undoubtedly the observation of a Higgs boson at mass around 125 GeV as reported by the ATLAS and CMS collaborations [16, 17]. With this major discovery and the excellent per-

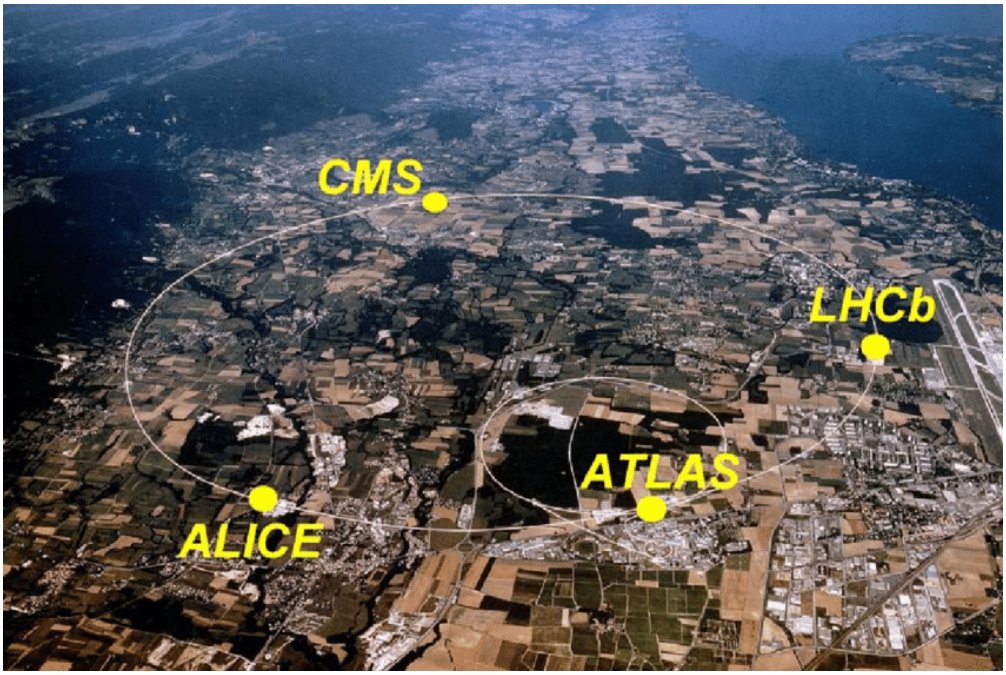

Figure 5: Satellite view of the LHC tunnel with the four detectors CMS, ALICE, ATLAS, and LHCb. Image: [15].

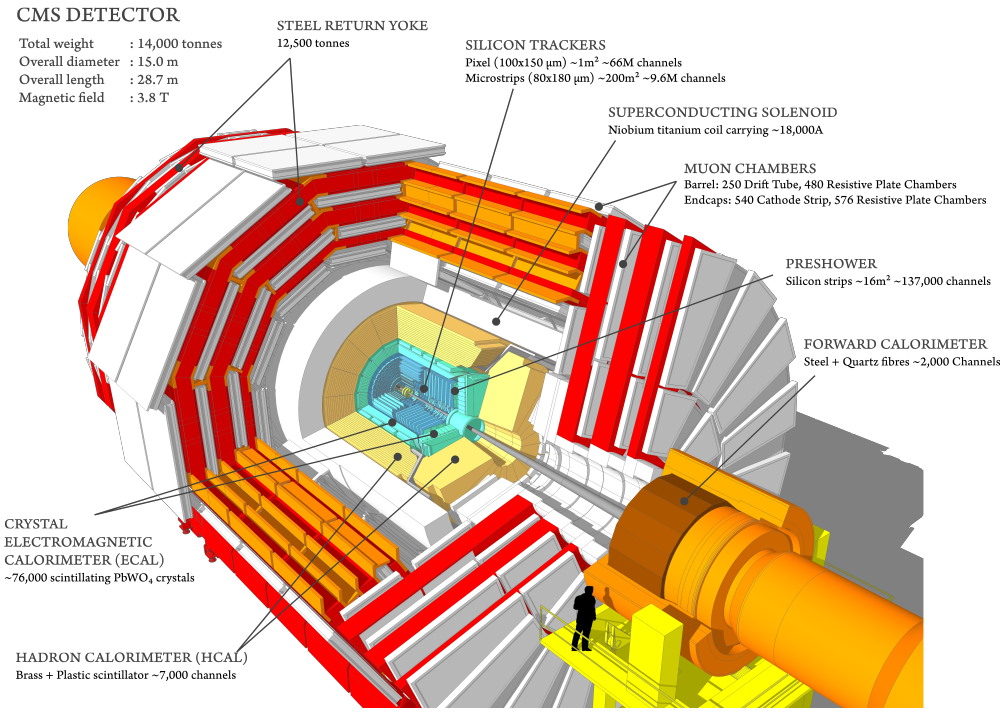

Figure 6: Structure and components of the Compact Muon Solenoid (CMS) detector. Image: [10]

formance of the LHC, the search for new phenomena at higher energy scales has intensified. While the discovery of new physics can be gleaned from precise measurements of interactions between Standard Model (SM) particles, the issues of the SM also motivate searching for new heavy particles predicted by theoretical extensions addressing its incompleteness. One outstanding issue is the so-called hierarchy problem related with the large difference in scale among the different interactions, i.e. that the electroweak scale is 16 orders of magnitude smaller than the Planck scale at which gravity becomes important. Various mechanisms have been proposed to solve the hierarchy problem. For example, modern theories which attempt to unify gravity with the SM postulate a solution to the hierarchy problem by assuming extra spatial dimensions through which gravity propagates [18]. While the extent of these theories is vast, the common result is the manifestation of new spin-2 bosons (Y_2) with TeV scale masses. In the so-called Randall-Sundrum (RS) model, these hypothetical particles are referred to as gravitons.

Previous LHC searches for spin-2 resonances were performed by the ATLAS [19] and CMS [20] collaborations using proton-proton (pp) collisions at $\sqrt{s} = 8$ and 13 TeV [21, 22, 23, 24, 25, 26]. Those results focused on Y_2 production via gluon-gluon (gg) fusion or quark-antiquark ($q\bar{q}$) annihilation (Fig. 7), followed by the Y_2 decay to a pair of photons ($\gamma\gamma$), leptons ($\ell\ell$), jets (jj), or heavy vector bosons (WW, ZZ). Although both collaborations reported the observation of a moderate excess of events compared to SM expectations near diphoton mass $m_{\gamma\gamma} = 750$ GeV with the 8 TeV pp data [21, 22], the 13 TeV results have shown no significant sign of new physics, resulting in exclusion bounds up to $m(Y_2) < 4$ TeV depending on the model [23, 24, 25]. However, exclusions depend strongly on the strength of the coupling between Y_2 and the quarks/gluons ($\kappa_{q,g}$). While previous searches typically assume more "natural" (SM-like) couplings (i.e. $\kappa_{q,g} = 1$), the lack of a strong excess thus far opens up the possibility that $\kappa_{q,g}$ is significantly smaller, in which case the Y_2 may have eluded discovery. If $\kappa_{q,g}$ is too small to provide large enough cross-section via the traditional

$gg \to Y_2$ or $q\bar{q} \to Y_2$ production mechanisms, another technique must be devised to probe Y_2.

In this analysis, we propose a search for a heavy spin-2 resonance produced through vector boson fusion (VBF) processes and decaying to a pair of photons (Fig. 8). The Y_2 production cross section from VBF processes is independent of $\kappa_{q,g}$. The identification of events produced via VBF processes has been a key experimental tool to the discovery of the Higgs boson [27]. The VBF topology has also been proposed as an effective tool for dark matter [28, 29], supersymmetry [30, 31, 32, 33, 34], Z' [35], and heavy neutrino searches at the LHC [36] due to the natural collinear logarithmic enhancement obtained in the production cross section at high mass values, as well as the significant reduction of SM backgrounds. The $Y_2 \to \gamma\gamma$ decay channel is motivated by its relatively clean experimental signature with localized diphoton mass spectrum. Furthermore, while spin-1 Z' and spin-2 Y_2 bosons can both result in dilepton, dijet, and ZZ/WW channels, an excess in the $\gamma\gamma$ final state would rule out a Z'.

To allow for a generic and model independent approach, we consider an effective field theory (EFT) consisting of three terms in the Lagrangian: (i) kinetic term $\mathcal{L}_{V,f} = -\frac{\kappa_{V,f}}{\Lambda} T^{V,f}_{\mu\nu} Y_2^{\mu\nu}$ representing the Y_2 interactions with the SM gauge (matter) fields V (f) and where $T^{V,f}_{\mu\nu}$ is the energy-momentum tensor of V or f; (ii) Y_2 interaction with the SM Higgs doublet Φ, $\mathcal{L}_\Phi = -\frac{\kappa_H}{\Lambda} T^{\Phi}_{\mu\nu} Y_2^{\mu\nu}$ with Φ energy-momentum tensor $T^{\Phi}_{\mu\nu}$; and (iii) Y_2 interactions with Fadeev-Popov (FP) ghost fields $\mathcal{L}_{\rm FP} = -\frac{\kappa_V}{\Lambda} T^{\rm FP}_{\mu\nu} Y_2^{\mu\nu}$, where $T^{\rm FP}_{\mu\nu}$ is the energy-momentum tensor of the FP ghost field. In the above Lagrangian equations Λ represents the cut-off scale, the gauge fields V are the SM electroweak gauge bosons or the gluon, and the matter fields f are quarks, leptons, and left-handed neutrinos. This particular implementation also allows for scenarios with non-universal couplings to be studied at NLO accuracy [37].

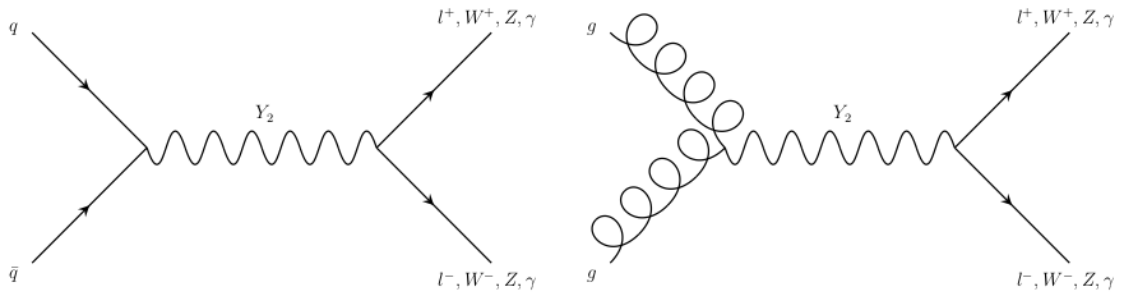

Figure 7: Representative Feynman diagrams depicting Y_2 production via quark-antiquark annihilation (left) and gluon-gluon fusion (right).

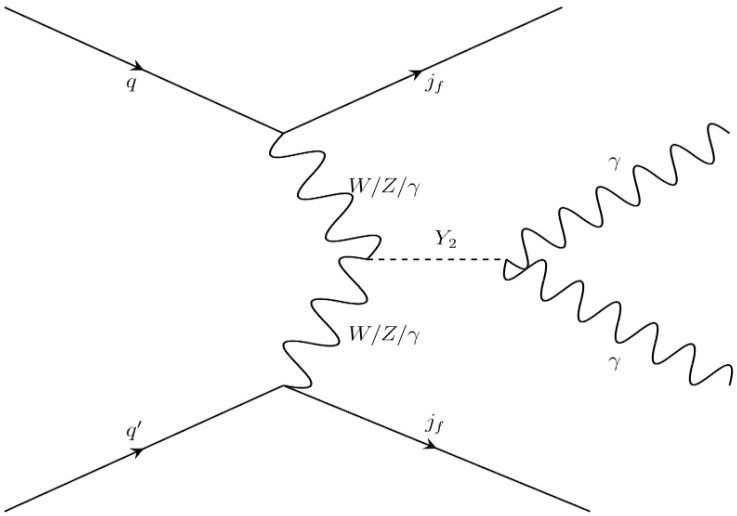

Figure 8: Representative Feynman diagrams depicting pure electroweak VBF production of a Y_2 particle and two forward jets. The spin-2 Y_2 decays to a pair of photons.

2 Samples and simulation

Signal and background samples were generated with MadGraph5_aMC (v2.6.4) [38], considering proton-proton (pp) beams with $\sqrt{s} = 13$ TeV. In the case of the spin-2 signal samples, the model files were generated using the FeynRules package [39] and obtained from Ref. [40]. The dominant contributions to the total Y_2 decay width are from the massive SM final states (i.e. $Y_2 \to t\bar{t}$, $Y_2 \to W^+W^-$, $Y_2 \to ZZ$, and $Y_2 \to HH$), with a dependence given by $\Gamma(Y_2 \to XX) \approx \kappa_X^2 \frac{m(Y_2)^3}{\Lambda^2}(1 - 4\frac{m(X)^2}{m(Y_2)^2})^{(2l+1)/2}$, where l is the angular momentum quantum number, $m(X)$ is the mass of the heavy particle X, and κ_X the coupling of X to Y_2. The term $(1 - 4\frac{m(X)^2}{m(Y_2)^2})^{(2l+1)/2}$ represents the kinematically allowed phase space, i.e. $4\frac{m(X)^2}{m(Y_2)^2} < 1$ and thus $m(Y_2) > 2m(X)$. Therefore, since we allow the possibility that Y_2 couples to all the heavy SM particles, we consider $m(Y_2)$ values above $2m(t) \approx 350$ GeV.

To illustrate the unitarity violating phase space (to be defined below), we consider two benchmark scenarios: (i) standard couplings to the fermions, gluons, and Higgs boson ($\frac{\kappa_{f,g,H}}{\Lambda} = 1$ TeV^{-1}), but with a varying coupling $\kappa_V = \kappa_{\gamma,W,Z}$ to the electroweak bosons; and (ii) suppressed couplings to the gluon and light quarks $q = u, d, s, c, b$ ($\frac{\kappa_{q,g}}{\Lambda} = 0$), but with free parameter κ_V. The latter case represents a proxy for our main interest in this paper, where the lack of a strong excess in $gg \to Y_2$ and $q\bar{q} \to Y_2$ searches thus far motivates the possibility that $\kappa_{q,g}$ is small. This scenario makes VBF an important mode for discovery. On the other hand, it is important to point out that even if $\kappa_{q,g} \approx 1$ (or larger), a VBF Y_2 search is still relevant to establish the coupling of Y_2 to the vector bosons of the SM, which is important to assess the correct physics model that best fits the observed data should there be evidence for discovery. To preserve unitarity, we require that the total decay width of Y_2 (calculated from Ref. [40]) cannot exceed the mass of Y_2. Fig. 9 shows the unitarity-violating phase space (i.e, where the total decay width of Y_2 exceeds $m(Y_2)$) and the $Y_2 \to \gamma\gamma$ branching ratio, as a function of $m(Y_2)$ and κ_V, for the benchmark case where we assume

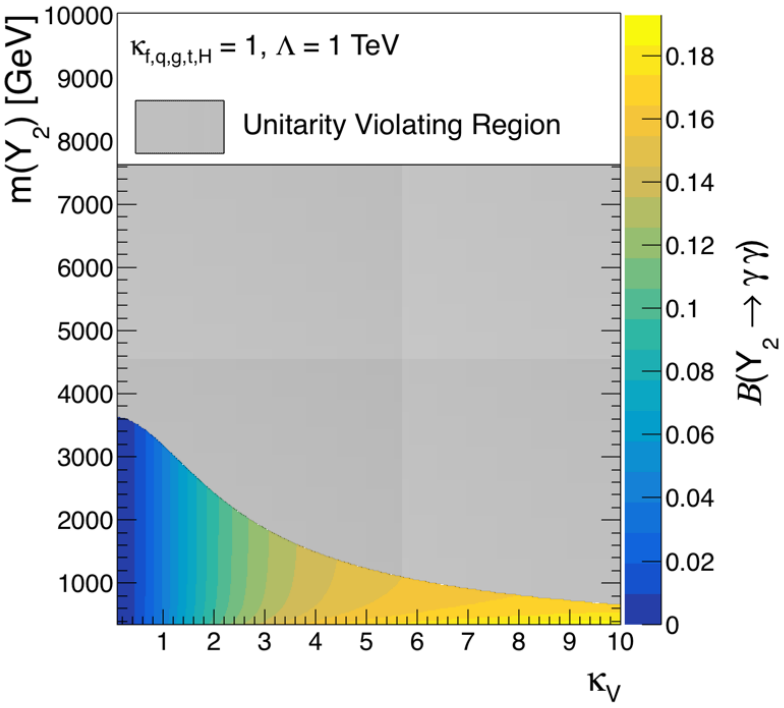

Figure 9: $Y_2 \to \gamma\gamma$ branching ratio as a function of $m(Y_2)$ and κ_V, for the benchmark case where $\kappa_{f,g,H} = 1$. The gray shaded region represents the unitarity-violating phase space.

$\kappa_{f,g,H} = 1$. Fig. 10 shows the unitarity-violating phase space and the $Y_2 \to \gamma\gamma$ branching ratio, as a function of $m(Y_2)$ and κ_V, for the benchmark case where we assume $\kappa_{q,g} = 0$. In the scenario with more natural couplings to the light quarks and gluon, the unitarity acceptable region extends to $m(Y_2) \approx 3.6$ (3.2) TeV for $\kappa_V = 0.1$ (1.0). The theoretically allowed region can be as large as $m(Y_2) \approx 8.4$ (5.0) TeV for $\kappa_V = 0.1$ (1.0) when $\kappa_{q,g} = 0$. For this reason we generate signal samples with $m(Y_2)$ values up to 8.4 TeV. The diphoton branching ratio $B(Y_2 \to \gamma\gamma)$ is approximately 10 (4)% for $\kappa_{q,g} = 0$ (1) and $\kappa_V = 1.0$, but can be as high as about 20% for large κ_V values.

The signal samples were produced considering electroweak production of Y_2 with two associated jets and suppressed QCD coupling (i.e. $pp \to jjY_2$ with α^0_{QCD}). Fig. 11 shows the VBF Y_2 production cross section as a function of $m(Y_2)$ for $\kappa_V = 0.1$, 1.0, and 5.0. As expected, the cross section scales as κ_V^2. Fig. 12 shows the $Y_2 \to \gamma\gamma$ decay width as a

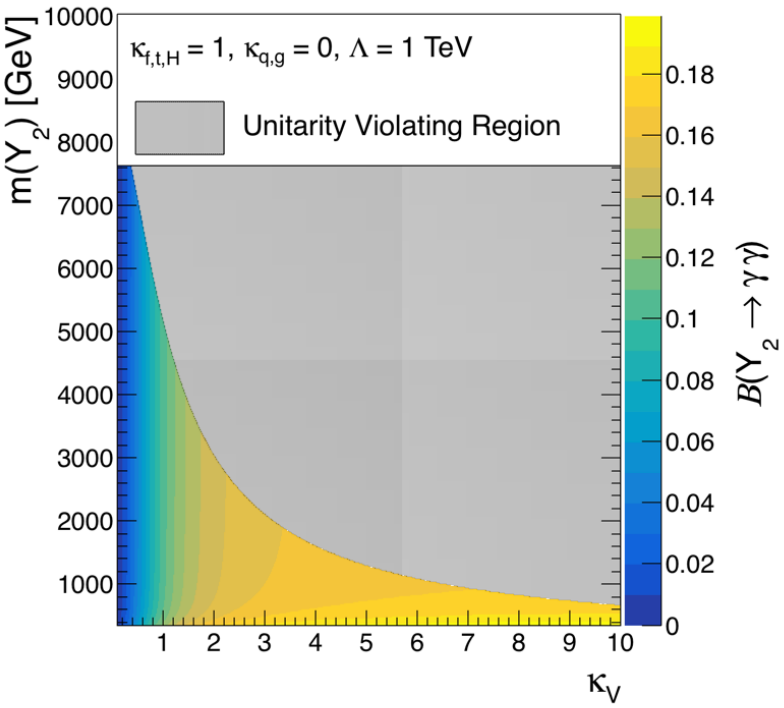

Figure 10: $Y_2 \to \gamma\gamma$ branching ratio as a function of $m(Y_2)$ and κ_V, for the benchmark case where $\kappa_{q,g} = 0$. The gray shaded region represents the unitarity-violating phase space.

function of $m(Y_2)$ for the three similar values of κ_V. The curves in Fig. 12 do not extend into the unitarity violating phase space.

The dominant sources of SM background are production of photon pairs with associated jets, referred to as $\gamma\gamma$+jets. In the proposed search region (defined in Section III), the associated jets are mainly from initial state radiation (i.e. $pp \to \gamma\gamma jj$, α^2_{QCD}) or SM VBF processes (i.e. $pp \to \gamma\gamma jj$, α^0_{QCD}). Therefore, the background samples are split into two categories: (i) non-VBF $\gamma\gamma$+jets events with up to four associated jets, inclusive in the electroweak coupling (α_{EWK}) and α_{QCD}; and (ii) pure electroweak VBF $\gamma\gamma jj$. The production of γ+jets and multijet events with jets misidentified as photons have been checked to provide a negligible contribution to the proposed search region due to the effectiveness of the VBF selection criteria. PYTHIA (v6.416) [41] was used for the hadronization process in both signal and background samples, while Delphes (v3.3.2) [42] was used to simulate detector effects using the CMS parameters. At MadGraph level, photons were required to have transverse momentum greater than 10 GeV and located in the central region of the ATLAS and CMS detectors ($|\eta(\gamma)| < 2.5$). Photon pairs were also required to be separated in η-ϕ space by requiring $\Delta R(\gamma_1, \gamma_2) = \sqrt{\Delta\phi(\gamma_1, \gamma_2)^2 + \Delta\eta(\gamma_1, \gamma_2)^2} > 0.4$. Similarly, at parton level the jets were required to have a minimum $p_T > 20$ GeV and $|\eta| < 5.0$. The MLM algorithm [43] was used for jet matching and jet merging. The xqcut and qcut variables of the MLM algorithm, related with the minimal distance between partons and the energy spread of the clustered jets, were set to 30 and 45 as result of an optimization process requiring the continuity of the differential jet rate as a function of jet multiplicity.

3 Event selection criteria

Although VBF processes are characterized by relatively low production cross sections (compared to DY and gluon-gluon fusion processes), the unique topology of VBF compensates for

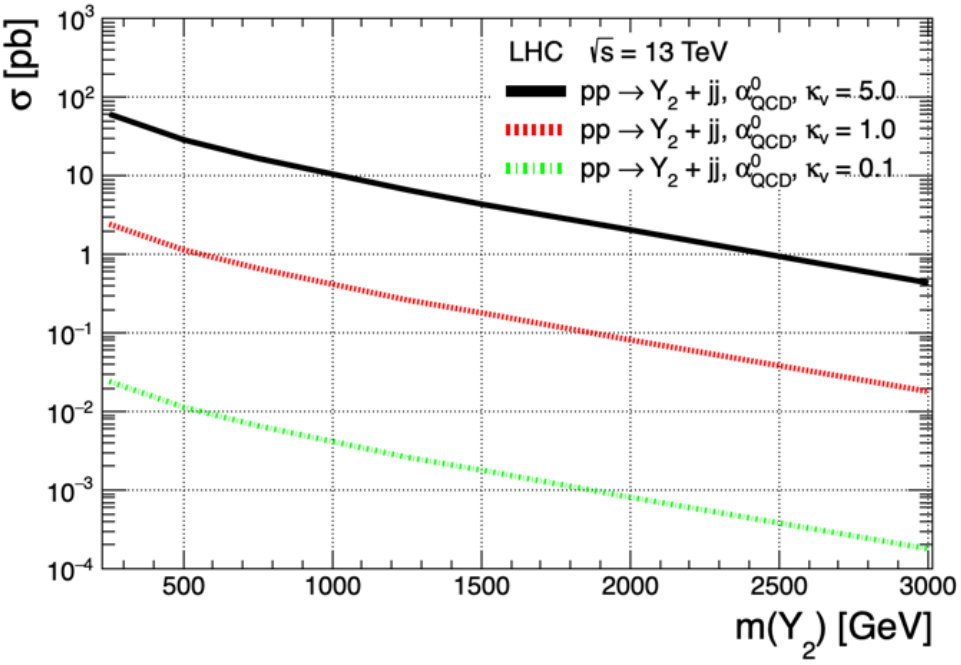

Figure 11: The VBF Y_2 cross-section as a function of $m(Y_2)$ and κ_V.

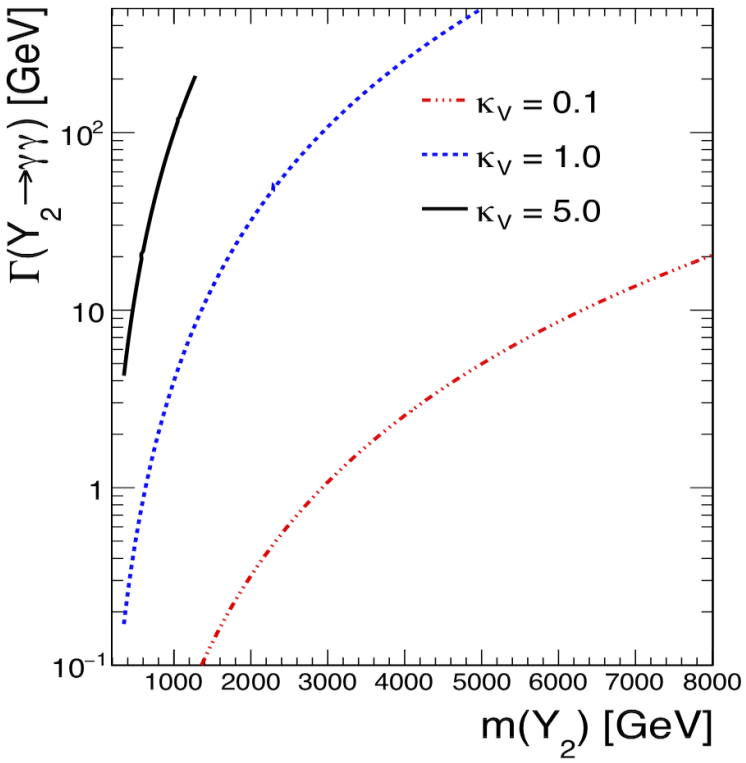

Figure 12: The $Y_2 \to \gamma\gamma$ decay width as a function of $m(Y_2)$ and κ_V.

Table 3: Event selection criteria.

Criterion	$\gamma_1\gamma_2 j_f j_f$
Central Selections	
$\lvert\eta(\gamma)\rvert, \lvert\eta(e)\rvert, \lvert\eta(\mu)\rvert, \lvert\eta(\tau_h)\rvert$	< 2.5
$\lvert\eta(\mathrm{b})\rvert$	< 2.4
$p_T(\gamma)$	> 30 GeV
$p_T(e), p_T(\mu)$	> 10 GeV
$p_T(\tau_h), p_T(\mathrm{b})$	> 20 GeV
$N(\gamma)$	$= 2$
$N(e), N(\mu), N(\tau_h), N(\text{b-jets})$	$= 0$
$p_T^{\mathrm{lead}}(\gamma)$	> 60 GeV
$\Delta R(\gamma_1, \gamma_2)$	> 0.4
VBF Selections	
$p_T(j)$	> 30 GeV
$\lvert\eta(j)\rvert$	< 5.0
$\Delta R(\gamma, j)$	> 0.4
$N(j)$	≥ 2
$\eta(j_1) \cdot \eta(j_2)$	< 0
$\lvert\Delta\eta(j_1, j_2)\rvert$	> 4.0 ("Loose")
	> 6.0 ("Tight")
m_{jj}	> 1.0 TeV

the smaller production rate by helping to significantly suppress SM backgrounds, especially those with jets arising from QCD interactions. The VBF topology consists of two high-p_T forward jets, in opposite sides of the detector, with a large difference in pseudorapidity and TeV scale dijet mass.

In the higher energy LHC environment, where $m(j) \ll p_T(j)$ and $E_T \approx p_T$, the dijet mass m_{jj} is well-approximated by $m_{jj} \approx \sqrt{2p_T^{j_1} p_T^{j_2} \cosh(\Delta\eta_{jj})}$. The transverse momentum requirement on the jets is driven by the experimental constraints of the CMS and ATLAS experiments. These constraints include the limitations of the reconstruction algorithms and the geometric acceptance of the detectors. Events are required to have at least two jets with $p_T(j) > 30$ GeV and $|\eta(j)| < 5.0$. Since m_{jj} depends on the p_T of each jet, we indirectly optimize the p_T values by optimizing m_{jj}. Considering the large pseudorapidity gap $|\Delta\eta_{jj}|$

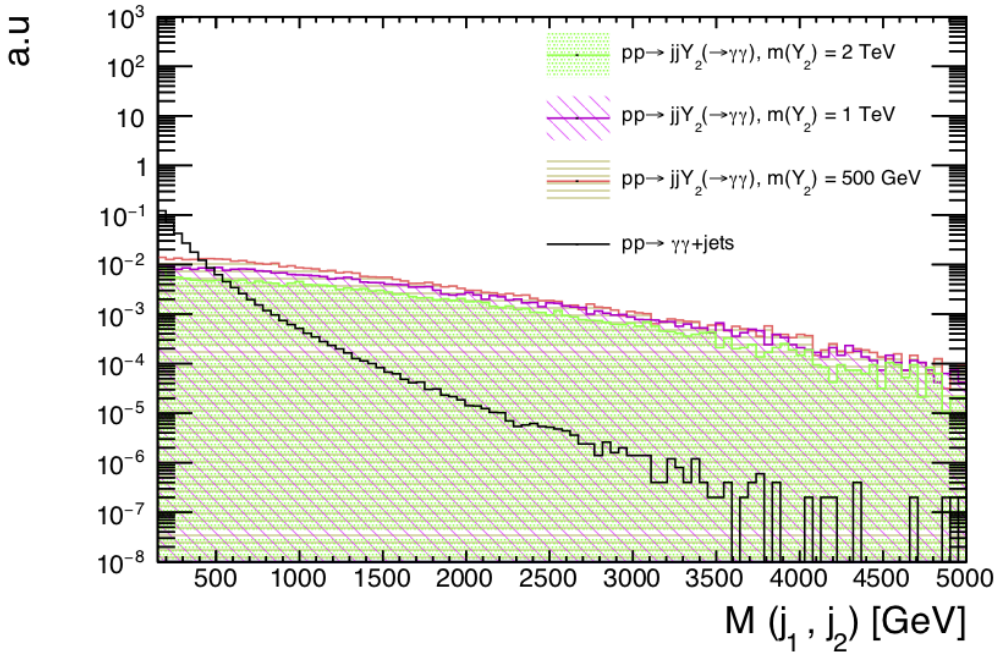

Figure 13: The dijet mass distribution (normalized to unity) for the total SM backgrounds and $m(Y_2) = 2$ TeV signal benchmark point.

in VBF Y_2 events, we impose a stringent requirement on the lower threshold of the calculated dijet mass.

Shown in Fig. 13 are the m_{jj} distributions (normalized to unity) of the total background and the signal benchmark point with $m(Y_2) = 2$ TeV. The signal distribution is broad and overtakes the SM backgrounds at TeV scale m_{jj}. The exact m_{jj} requirement, $m_{jj} > 1$ TeV, is determined through an optimization process that maximizes signal significance. For this purpose we take a simple approach to defining signal significance as $N_{\rm S}/\sqrt{N_{\rm S} + N_{\rm B} + (0.25N_{\rm B})^2}$, where $N_{\rm S}$ and $N_{\rm B}$ are the signal and background yields, respectively, while the factor of $0.25N_{\rm B}$ represents a 25% systematic uncertainty on the background (to be discussed later). The values of $N_{\rm S}$ and $N_{\rm B}$ in the optimization process are derived within a diphoton mass window $m(Y_2) - 2\Gamma < m_{\gamma\gamma} < m(Y_2) + 2\Gamma$, where Γ is the $Y_2 \to \gamma\gamma$ decay width. We note these particular definitions of $N_{\rm S}$, $N_{\rm B}$, and significance are used only for the purpose of optimizing the selections. We propose to determine final discovery potential with a shape based

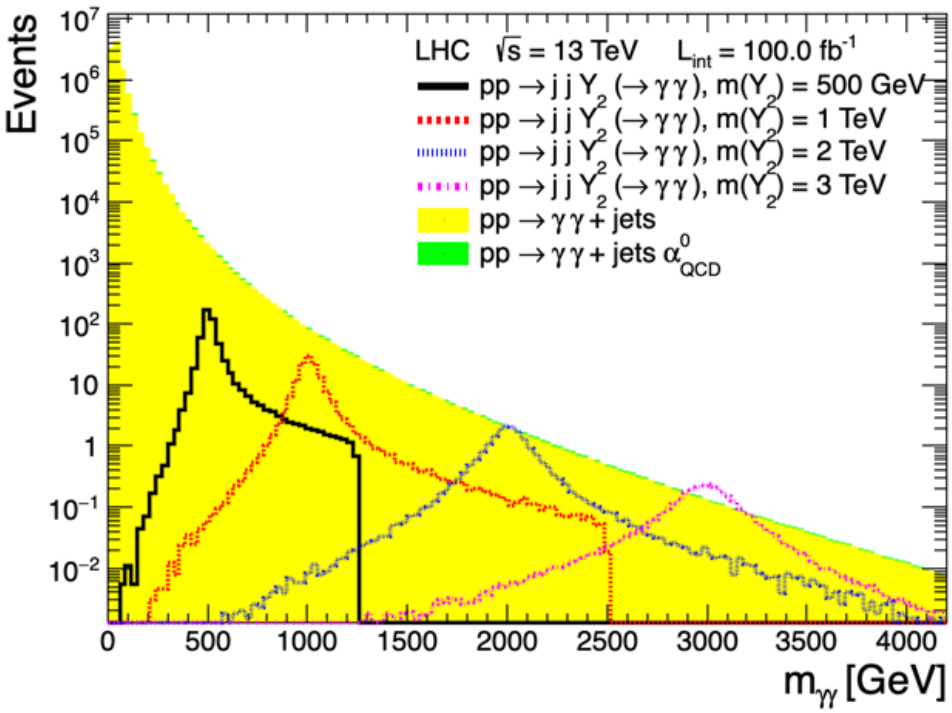

Figure 14: $m_{\gamma\gamma}$ distributions for the main backgrounds and various signal benchmark points. Simulated events populating these distributions have satisfied the requirements of at least two jets and two photons. A comparison of the signal and background distributions indicate the need to apply more stringent VBF selections for the low-mass signal benchmark points than the high-mass scenarios.

analysis to be described later in Section 4.

The optimal selection cut for the pseudorapidity gap $|\Delta\eta_{jj}|$ depends on $m(Y_2)$. Fig. 14 shows the distribution of the reconstructed diphoton mass ($m_{\gamma\gamma}$) for the main backgrounds and various signal benchmark points. The contribution from SM backgrounds decreases exponentially as $m_{\gamma\gamma}$ increases. On the other hand, the $m_{\gamma\gamma}$ signal distribution appears as a localized bump centered at approximately $m(Y_2)$. Since the signal benchmark points with small $m(Y_2)$ have low values of reconstructed $m_{\gamma\gamma}$ lying within the bulk of the background distributions, a more stringent $|\Delta\eta_{jj}|$ cut is required to efficiently reduce the SM backgrounds. The signal benchmark points with high $m(Y_2)$ values, on the other hand, lie in the tail of the reconstructed $m_{\gamma\gamma}$ background distribution, thus requiring a less stringent $|\Delta\eta_{jj}|$ cut.

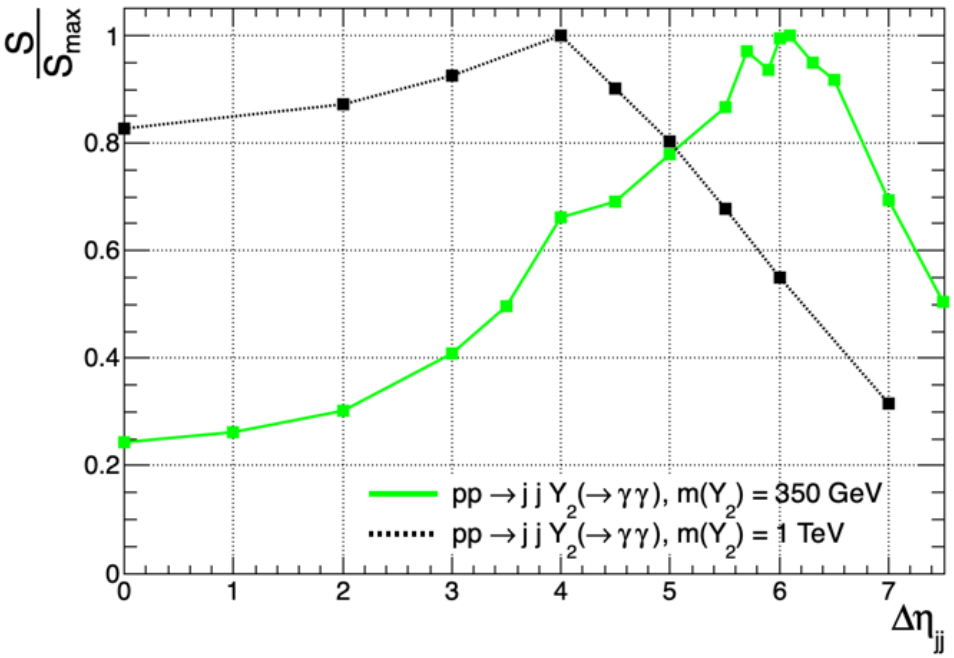

Figure 15: The normalized signal significance $\frac{S}{S_{\max}}$ as a function of the lower bound imposed on $|\Delta\eta_{jj}|$. The critical point at 6.0 for $m(Y_2) = 350$ GeV motives us to apply a "Tight" selection cut of $|\Delta\eta| > 6.0$ to maximize discovery potential for low mass signal models. Similarly, the critical point at 4.0 for $m(Y_2) = 1$ TeV motives us to apply a "Loose" selection cut of $|\Delta\eta| > 4.0$ to maximize discovery potential for high mass (TeV scale) signal models.

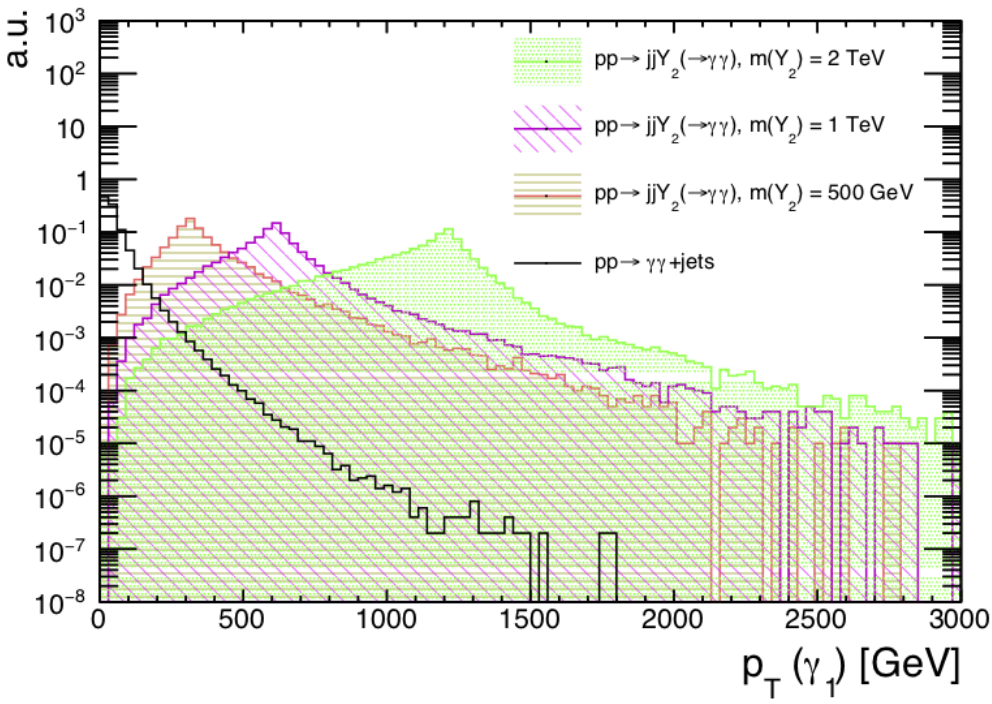

Figure 16: $p_T^{\text{lead}}(\gamma)$ distributions, normalized to unity, for the main backgrounds and various signal benchmark points.

Fig. 15 shows the normalized signal significance S/S_{max} as a function of $|\Delta\eta_{jj}|$ cut value, assuming an integrated luminosity of 100 fb^{-1}. The normalized significance is the significance at a given cut value, divided by the maximum significance over all possible cut values of the variable under study. The signal significance for $m(Y_2) = 350$ GeV is maximized with $|\Delta\eta_{jj}| > 6.0$, while $|\Delta\eta_{jj}| > 4.0$ provides the best discovery potential for the higher mass signal point $m(Y_2) = 1$ TeV. We hence define a "Tight" and "Loose" signal region with pseudorapidity gap requirements of $|\Delta\eta_{jj}| > 6.0$ and $|\Delta\eta_{jj}| > 4.0$, respectively, in an attempt to maximize the sensitivity to low and high mass signatures. The results shown in Section 4 are obtained by applying both "Tight" and "Loose" criteria and choosing the one that gives the largest signal significance for a given $m(Y_2)$ value.

In addition to the VBF selections, we select two γ candidates, requiring that $p_T(\gamma) > 30$ GeV and $|\eta(\gamma)| < 2.5$ for both photons with $p_T^{\text{lead}}(\gamma) > 60$ GeV for the leading photon.

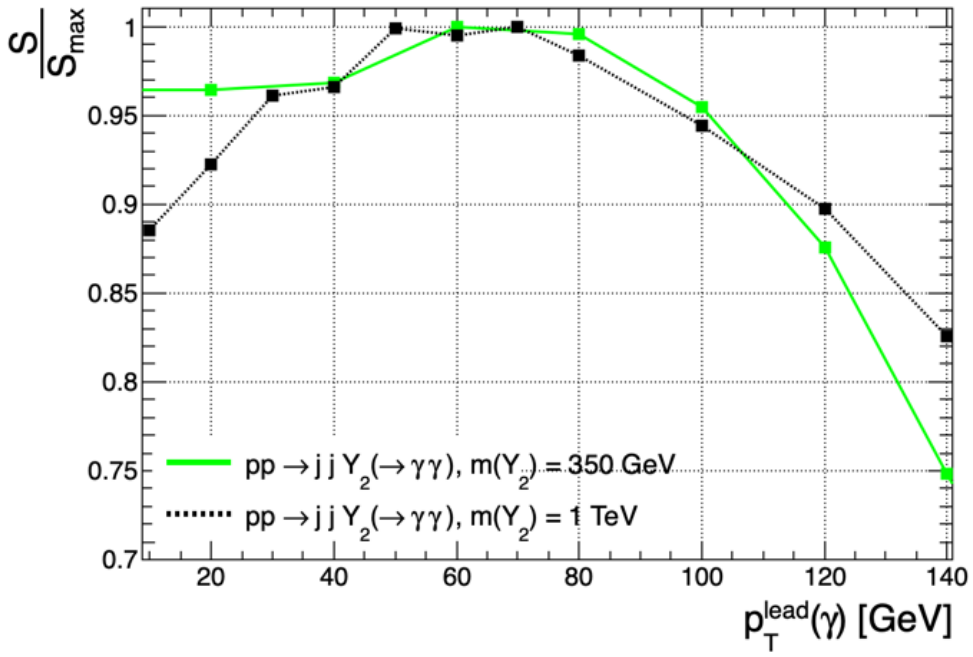

Figure 17: The normalized signal significance $\frac{S}{S_{\max}}$ as a function of the lower bound imposed on $p_T^{\text{lead}}(\gamma)$. The signal significance is maximized at around around 60 GeV for both benchmark points with $m(Y_2) = 350$ GeV and $m(Y_2) = 1$ TeV, which motives a selection cut at $p_T^{\text{lead}}(\gamma) > 60$ GeV.

The signal and background p_T distributions (normalized to unity) of the leading photon are shown in Fig. 16, while Fig. 17 shows the normalized signal significance $S/S_{\max}$ as a function of $p_T^{\text{lead}}(\gamma)$ cut value, assuming an integrated luminosity of 100 fb^{-1}. The signal significance is maximized at approximately 60 GeV for both the $m(Y_2) = 350$ GeV and the $m(Y_2) = 1$ TeV benchmark points, which supports our choice of selection cut at $p_T^{\text{lead}}(\gamma) > 60$ GeV. By a similar methodology, we determined the optimal threshold for the p_T of the sub-leading photon to be $p_T(\gamma) > 30$ GeV.

Finally, in addition to the VBF dijet and diphoton selections, simulated events in the proposed search region are required to have zero jets tagged as b-quarks and no reconstructed/identified leptons (electrons, muons, or hadronically decaying taus). While these selections are highly efficient for VBF $Y_2 \to \gamma\gamma$ signal events ($> 90\%$), they simultaneously help to ensure the negligible contribution from SM backgrounds with top quarks, pairs of vector bosons, $Z/\gamma* \to \ell\ell$ with associated jets, and $W \to \ell\nu$ with associated jets. Electrons and muons used in the lepton veto requirement must have $p_T > 10$ GeV and $|\eta| < 2.5$, while hadronically decaying tau leptons (τ_h) have $p_T > 20$ GeV and $|\eta| < 2.5$. Similarly, b-jets are defined by $p_T > 20$ GeV and $|\eta| < 2.4$. The difference in the τ_h/b-jet p_T thresholds, in comparison to the electron/muon thresholds, is due to the experimentally more challenging nature of τ_h and b-jet reconstruction. The event selection criteria used in the $\gamma_1\gamma_2 j_f j_f$ "Tight" and "Loose" signal regions are summarized in Table 3.

Fig. 18 shows the signal and background $m_{\gamma\gamma}$ distributions, after applying the "Loose" event selection criteria as listed in Table 3 with $|\Delta\eta| > 4.0$. Fig. 19 is similar but with the "Tight" $|\Delta\eta|$ requirement of 6.0. Again, the bulk of the (now largely reduced) background distribution lies at relatively low reconstructed diphoton mass values, while the signal bumps dominate at the tails of the $m_{\gamma\gamma}$ distribution. Depending on the $\Delta\eta$ cut value, the contributions of the $\gamma\gamma$+jets backgrounds are reduced by approximately 4-5 orders of magnitude, while the signal acceptance is 12-58% depending on $m(Y_2)$.

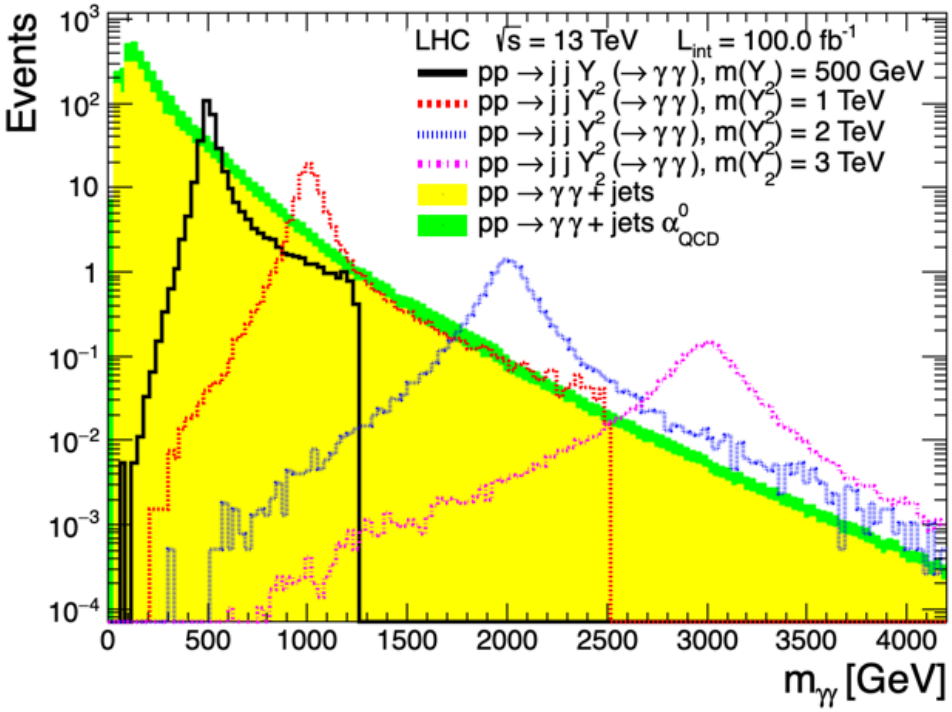

Figure 18: $m_{\gamma\gamma}$ distribution for the main backgrounds and various signal benchmark points, after applying the event selection criteria as in Table 3 with $|\Delta\eta| > 4.0$.

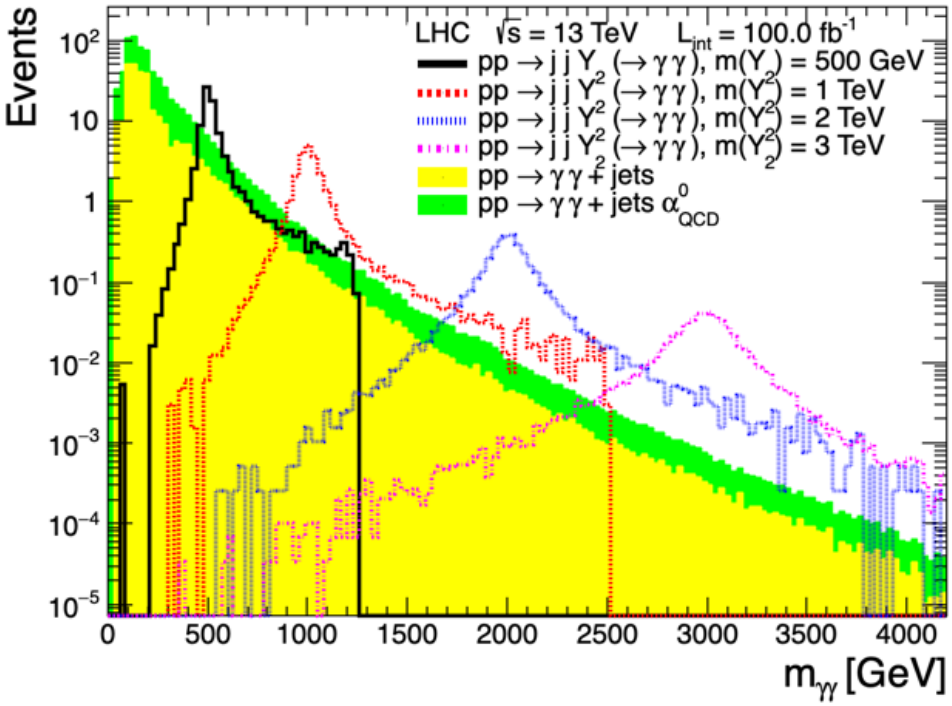

Figure 19: $m_{\gamma\gamma}$ distribution for the main backgrounds and various signal benchmark points, after applying the event selection criteria as in Table 3 with $|\Delta\eta| > 6.0$.

4 Results

We use the full range of the reconstructed diphoton mass distribution to perform a shape based analysis of the discovery potential, following a profile binned likelihood approach to define the test statistic, using the ROOFit [44] toolkit. Systematic uncertainties are incorporated into the calculation as nuisance parameters in order to obtain an experimentally realistic estimate of the signal significance. A 15% systematic uncertainty related with γ identification efficiency, based on [21, 22], has been included, considering 100% correlation between the two photons and 100% correlation among signal and background processes. In addition, a 12% uncertainty in the signal and background yields due to the choice of parton distribution function (PDF) included in the simulated signal samples is evaluated based on the PDF4LHC recommendations [45]. This is consistent with the 15% uncertainty from the CMS VBF SUSY and VBF dark matter searches [29, 34]. The effect of the chosen PDF set on the shape of the $m_{\gamma\gamma}$ distribution is negligible. Finally, we have included a 20% uncertainty related with the experimental difficulties involved with reconstructing, identifying, and calibrating forward jets at the LHC. This 20% effect is categorized as an overall uncertainty on the efficiency of the VBF selection criteria, based on Refs. [29, 34]. A local p-value is calculated as the probability under a background only hypothesis to obtain a value of the test statistic as large as that obtained with a signal plus background hypothesis. The signal significance S is then defined as the value at which the integral of a Gaussian between S and ∞ results in a value equal to the local p-value.

The expected signal significance has been calculated considering different scenarios of integrated luminosity at the LHC, ranging from 100 to 3000 fb^{-1} (based on the current and projected luminosity at the LHC), and assuming different values of κ_V. The results are presented in Figs. 20 and 21, as $m(Y_2)$ vs. κ_V on the $y-x$ plane, and the expected signal significance (using the shape based approach) on the $z-$axis. Similar to Figs. 9- 10, only

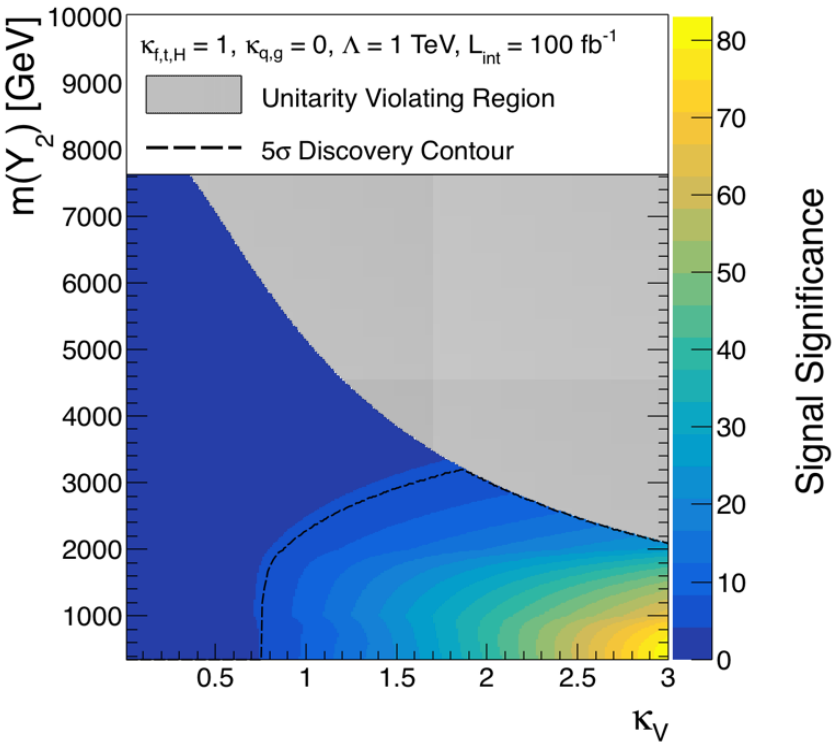

Figure 20: Expected signal significance for the proposed VBF final state. The results are shown as $m(Y_2)$ vs. κ_V on the $y-x$ plane, and the expected signal significance on the $z-$axis. The expected signal significance was calculated performing a profile binned likelihood of the diphoton mass distribution, assuming an expected luminosity of 100 fb^{-1}. The black dashed line encloses the region with 5σ discovery potential.

the unitarity acceptable region $\Gamma < m(Y_2)$ in the EFT is considered for the calculation of the signal significances. The black dashed line in Figs. 20 and 21 delimits the 5σ discovery contour. Assuming an integrated luminosity of 100 fb^{-1} (3000 fb^{-1}), there is discovery potential for $\kappa_V > 1.85$ (1.7) in the entire range of theoretically allowed values for $m(Y_2)$ (up to 4.4 TeV). For lower couplings of $\kappa_V = 0.6$ (1.0), the proposed VBF $Y_2 \to \gamma\gamma$ search can provide signal significances greater than 5σ for Y_2 masses up to 3.0 (4.2) TeV with the amount of pp data expected from the high-luminosity LHC.

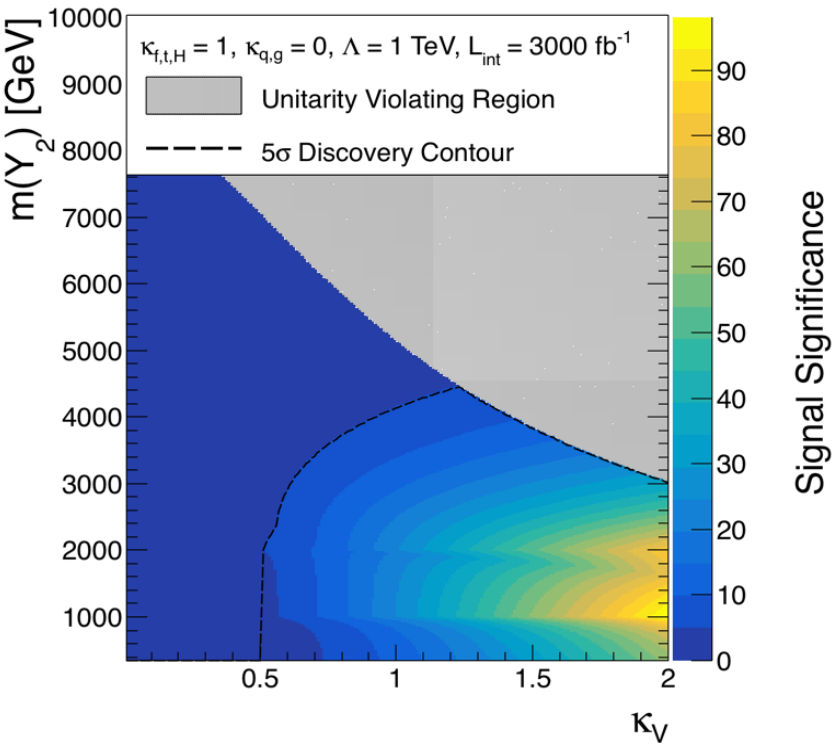

Figure 21: Expected signal significance for the proposed VBF final state. The results are shown as $m(Y_2)$ vs. κ_V on the $y-x$ plane, and the expected signal significance on the $z-$axis. The expected signal significance was calculated performing a profile binned likelihood of the diphoton mass distribution, assuming an expected luminosity of 3000 fb^{-1}. The black dashed line encloses the region with 5σ discovery potential.

5 Discussion

The main result of this paper is that probing heavy spin-2 bosons Y_2 produced through VBF processes can be a key methodology to complement current searches for TeV scale particles at the LHC. In the context of a generic and model independent approach via an effective field theory, both standard and non-universal couplings for Y_2 to the SM particles can be studied. Of particular interest is that there has been no evidence for a TeV scale Y_2 at the LHC to date. The Y_2 boson may have failed to be discovered in searches within the CMS and ATLAS experiments thus far because $\kappa_{q,g}$ is small. Thus, the Y_2 would not be discoverable by the "standard" searches via gluon-gluon fusion or quark-antiquark annihilation currently conducted at the LHC. In addition, even if a Y_2 were to be discovered with $gg \to Y_2$ or $q\bar{q} \to Y_2$, a VBF Y_2 search remains a key part of the Y_2 search program at the LHC in order to establish the couplings κ_V of the Y_2 to the SM vector bosons. We consider Y_2 decays to $\gamma\gamma$ to show that the requirement of a diphoton pair combined with two high p_T forward jets with large separation in pseudorapidity and with large dijet mass is effective in reducing contributions from QCD multijet, γ+jets, $\gamma\gamma$+jets, and other SM backgrounds. Dilepton, dijet, and ZZ/WW channels can all result from spin-1 Z' or spin-2 Y_2 production. However, an excess in the $\gamma\gamma$ final state would rule out Z'. In keeping within the EFT in this analysis, various values of κ_V have been studied, and effects of varying κ_V on the branching ratio and decay width for Y_2 have been considered. These considerations related to κ_V have been made with particular attention to the theoretically allowed phase space for determining discovery potential. Assuming proton-proton collisions at $\sqrt{s} = 13$ TeV, the proposed VBF $Y_2 \to \gamma\gamma$ search is expected to achieve a discovery reach with signal significance greater than 5σ for Y_2 masses up to 4.4 TeV and κ_V couplings down to 0.5.

References

[1] "Planck — Dark Matter, Dark Energy, Dark Gravity," https://darkmatterdarkenergy.com/tag/planck/

[2] "Strong interaction," https://en.wikipedia.org/wiki/Strong_interaction

[3] "The Four Forces - Range and Force Carriers," http://webhome.phy.duke.edu/~kolena/modern/forces.html#005

[4] University of Zurich, "Standard Model," https://www.physik.uzh.ch/en/researcharea/lhcb/outreach/StandardModel.html

[5] D. Griffiths, "Introduction to elementary particles; 2nd rev. version," Wiley, New York, NY. 2008.

[6] Glenn Elert, "The Physics Hypertextbook - The Standard Model," https://physics.info/standard/

[7] "Higgs boson," https://en.wikipedia.org/wiki/Higgs_boson

[8] CERN, "The Higgs boson," https://home.cern/science/physics/higgs-boson

[9] https://marketbusinessnews.com/physics-may-have-reached-its-limit-says-eminent-scien
120652/

[10] "DETECTOR," https://cms.cern/detector

[11] "The Large Hadron Collider," https://home.cern/science/accelerators/large-hadron-collider

[12] "Large Hadron Collider," https://en.wikipedia.org/wiki/Large_Hadron_Collider

[13] "LHC Report: Back in production," https://home.cern/news/news/accelerators/lhc-report-back-production

[14] Xabier Cid Vidal and Ramon Cid Manzano, "Luminosity - Taking a closer look at LHC," https://www.lhc-closer.es/taking_a_closer_look_at_lhc/0.luminosity

[15] Costanza Cavicchioli and L. Masotti and Elena Biagi and Davide Bozzini, "Fault detection on the Large Hadron Collider at CERN: design, simulation and realization of a High Voltage Pulse Generator," https://www.researchgate.net/publication/40534612_Fault_detection_on_the_Large_Hadron_Collider_at_CERN_design_simulation_and_realization_of_a_High_Voltage_Pulse_Generator

[16] G. Aad *et al.* [ATLAS Collaboration], "Observation of a new particle in the search for the Standard Model Higgs boson with the ATLAS detector at the LHC," Phys. Lett. B **716**, 1, 1-29 (2012) 10.1016/j.physletb.2012.08.020 [arXiv:1207.7214 [hep-ex]].

[17] V. Khachatryan *et al.* [CMS Collaboration], "Observation of a new boson at a mass of 125 GeV with the CMS experiment at the LHC," Phys. Lett. B **716**, 1, 30-61 (2012) 10.1016/j.physletb.2012.08.021 [arXiv:1207.7235 [hep-ex]].

[18] L. Randall and R. Sundrum, Phys. Rev. Lett. **83**, 3370 (1999) doi:10.1103/PhysRevLett.83.3370 [hep-ph/9905221].

[19] G. Aad *et al.* [ATLAS Collaboration], "The ATLAS Experiment at the CERN Large Hadron Collider," JINST **3**, S08003 (2008). doi:10.1088/1748-0221/3/08/S08003

[20] S. Chatrchyan *et al.* [CMS Collaboration], "The CMS experiment at the CERN LHC," JINST **3**, S08004 (2008). doi:10.1088/1748-0221/3/08/S08004

[21] V. Khachatryan *et al.* [CMS Collaboration], "Search for resonant production of high-mass photon pairs in proton-proton collisions at $\sqrt{s} = 8$ and 13 TeV," Phys. Rev. Lett. **117**, 051802 (2016) doi:10.1103/PhysRevLett.117.051802 [arXiv:1606.04093v2 [hep-ex]].

[22] M. Aaboud *et al.* [ATLAS Collaboration], "Search for high-mass diphoton resonances in *pp* collisions at $\sqrt{s}$=8 TeV with the ATLAS detector," Phys. Rev. D **92**, 032004 (2015) doi:10.1103/PhysRevD.92.032004 [arXiv:1504.05511v2 [hep-ex]].

[23] V. Khachatryan *et al.* [CMS Collaboration], "Search for high-mass diphoton resonances in proton-proton collisions at 13 TeV and combination with 8 TeV search," Phys. Lett. B **767**, 147 (2017) doi:10.1016/j.physletb.2017.01.027 [arXiv:1609.02507v2 [hep-ex]].

[24] M. Aaboud *et al.* [ATLAS Collaboration], "Search for resonances in diphoton events at $\sqrt{s}$=13 TeV with the ATLAS detector," JHEP **1609**, 001 (2016) doi:10.1007/JHEP09(2016)001 [arXiv:1606.03833 [hep-ex]].

[25] M. Aaboud *et al.* [ATLAS Collaboration], "Search for new phenomena in high-mass diphoton final states using 37 fb^{-1} of proton?proton collisions collected at $\sqrt{s}$=13 TeV with the ATLAS detector," Phys. Lett. B **775**, 105 (2017) doi:10.1016/j.physletb.2017.10.039 [arXiv:1707.04147v3 [hep-ex]].

[26] V. Khachatryan *et al.* [CMS Collaboration], "Search for a heavy resonance decaying to a pair of vector bosons in the lepton plus merged jet final state at $\sqrt{s} = 13$ TeV," JHEP **05**, 088 (2018) doi:10.1007/JHEP05(2018)088 [arXiv:1802.09407v2 [hep-ex]].

[27] V. Khachatryan *et al.* [CMS Collaboration], "Observation of the Higgs boson decay to a pair of tau leptons with the CMS detector," Phys. Lett. B **779**, 283 (2018) doi:10.1016/j.physletb.2018.02.004 [arXiv:1708.00373v2 [hep-ex]].

[28] A. Delannoy *et al.*, "Probing Dark Matter at the LHC using Vector Boson Fusion Processes," Phys. Rev. Lett. **111**, 061801 (2013) doi:10.1103/PhysRevLett.111.061801 [arXiv:1304.7779 [hep-ph]].

[29] V. Khachatryan *et al.* [CMS Collaboration], "Search for dark matter and supersymmetry with a compressed mass spectrum in the vector boson fusion topology in proton-proton collisions at $\sqrt{s} = 8$ TeV," Phys. Rev. Lett. **118**, 021802 (2017) 10.1103/PhysRevLett.118.021802 [arXiv:1605.09305v2 [hep-ex]].

[30] B. Dutta, A. Gurrola, W. Johns, T. Kamon, P. Sheldon and K. Sinha, "Vector Boson Fusion Processes as a Probe of Supersymmetric Electroweak Sectors at the LHC," Phys. Rev. D **87**, no. 3, 035029 (2013) doi:10.1103/PhysRevD.87.035029 [arXiv:1210.0964 [hep-ph]].

[31] B. Dutta, T. Ghosh, A. Gurrola, W. Johns, T. Kamon, P. Sheldon, K. Sinha and S. Wu, "Probing Compressed Sleptons at the LHC using Vector Boson Fusion Processes," Phys. Rev. D **91**, 055025 (2015) 10.1103/PhysRevD.91.055025 [arXiv:1411.6043 [hep-ph]].

[32] B. Dutta, W. Flanagan, A. Gurrola, W. Johns, T. Kamon, P. Sheldon, K. Sinha, K. Wang and S. Wu, "Probing Compressed Top Squarks at the LHC at 14 TeV," Phys. Rev. D **90**, 095022 (2014) 10.1103/PhysRevD.90.095022 [arXiv:1312.1348 [hep-ph]].

[33] B. Dutta *et al.*, "Probing Compressed Bottom Squarks with Boosted Jets and Shape Analysis," Phys. Rev. D **92**, 095009 (2015) 10.1103/PhysRevD.92.095009 [arXiv:1507.01001 [hep-ph]].

[34] V. Khachatryan *et al.* [CMS Collaboration], "Search for supersymmetry in the vector-boson fusion topology in proton-proton collisions at $\sqrt{s} = 8$ TeV," JHEP **1511**, 189 (2015) doi:10.1007/JHEP11(2015)189 [arXiv:1508.07628 [hep-ex]].

[35] A. Florez, A. Gurrola, W. Johns, Y. Oh, P. Sheldon, D. Teague, and T. Weiler, "Searching for New Heavy Neutral Gauge Bosons using Vector Boson Fusion Processes at the LHC," Phys. Lett. B **767**, 126-132 (2017) doi:10.1016/j.physletb.2017.01.062 [arXiv:1609.09765v2 [hep-ph]].

[36] A. Florez, A. Gurrola, K. Gui, C. Patino, and D. Restrepo, "Expanding the Reach of Heavy Neutrino Searches at the LHC," Phys. Lett. B **778**, 94-100 (2018) doi:10.1016/j.physletb.2018.01.009 [arXiv:1708.03007v1 [hep-ph]].

[37] G. Das, C. Degrande, V. Hirschi, F. Maltoni, and H. Shao, "NLO predictions for the production of a spin-two particle at the LHC," Phys. Lett. B **770**, 507-513 (2017) doi:10.1016/j.physletb.2017.05.007 [arXiv:1605.09359v2 [hep-ph]].

[38] J. Alwall *et al.*, "The automated computation of tree-level and next-to-leading order differential cross sections, and their matching to parton shower simulations," JHEP **1407**, 079 (2014) doi:10.1007/JHEP07(2014)079 [arXiv:1405.0301 [hep-ph]].

[39] N. D. Christensen, and C. Duhr, "FeynRules - Feynman rules made easy," Comput. Phys. Commun. **180**, 1614-1641 (2009) doi:10.1016/j.cpc.2009.02.018 [arXiv:0806.4194 [hep-ph]].

[40] doi:http://feynrules.irmp.ucl.ac.be/wiki/NLOModels.

[41] T. Sjostrand, S. Mrenna and P. Z. Skands, J. High Energy Phys. **0605**, 026 (2006) [hep-ph/0603175].

[42] J. de Favereau *et al.* [DELPHES 3 Collaboration], "DELPHES 3, A modular framework for fast simulation of a generic collider experiment," JHEP **1402**, 057 (2014) doi:10.1007/JHEP02(2014)057

[43] J. Alwall *et al.*, "Comparative study of various algorithms for the merging of parton showers and matrix elements in hadronic collisions," Eur. Phys. J. C 53, 473 (2008) doi:10.1140/epjc/s10052-007-0490-5, arXiv:0706.2569.

[44] L. Moneta, K. Belasco, K. S. Cranmer, S. Kreiss, A. Lazzaro, et. al., The RooStats Project, PoS ACAT2010 (2010) 057, [1009.1003]

[45] J. Butterworth *et al.*, "PDF4LHC recommendations for LHC Run II," J. Phys. G **43**, 023001 (2016) doi:10.1088/0954-3899/43/2/023001 [arXiv:1510.03865 [hep-ph]].